REPORT DOCUMENTATION PAGE

Form Approved OMB No. 0704-0188

Public reporting burden for this collection of information is estimated to average 1 hour per response, including the time for reviewing instructions, searching existing data sources, gathering and maintaining the data needed, and completing and reviewing the collection of information. Send comments regarding this burden estimate or any other aspect of this collection of information, including suggestions for reducing this burden to Washington Headquarters Services, Directorate for Information Operations and Reports, 1215 Jefferson Davis Highway, Suite 1204, Arlington, VA 22202-4302, and to the Office of Management and Budget, Paperwork Reduction Project (0704-0188), Washington, DC 20503.

1. AGENCY USE ONLY (Leave blank)	2. REPORT DATE	3. REPORT TYPE AND DATES COVERED
		Final Report

4. TITLE AND SUBTITLE

'Infrared Focal Plane Arrays Based on Semiconductor Quantum Dots'

5. FUNDING NUMBERS

F61775-00-WE

6. AUTHOR(S)

Prof. Eliezer Finkman

7. PERFORMING ORGANIZATION NAME(S) AND ADDRESS(ES)

Technion Research Authority
Haifa 3200
Israel

8. PERFORMING ORGANIZATION REPORT NUMBER

N/A

9. SPONSORING/MONITORING AGENCY NAME(S) AND ADDRESS(ES)

EOARD
PSC 802 BOX 14
FPO 09499-0200

10. SPONSORING/MONITORING AGENCY REPORT NUMBER

SPC 00-4048

11. SUPPLEMENTARY NOTES

12a. DISTRIBUTION/AVAILABILITY STATEMENT

Approved for public release; distribution is unlimited.

12b. DISTRIBUTION CODE

A

13. ABSTRACT (Maximum 200 words)

This report results from a contract tasking Technion Research Authority as follows: The contractor will investigate the feasibility of implementing quantum dot infrared photodetectors (QDIP) for operation in the mid- and long-infrared regions. It is expected that much better signal-to-noise ratio will be obtained, and normal incidence detection will be possilble.

14. SUBJECT TERMS

EOARD, Sensor Technology, Semiconductor materials, Focal plane arrays

15. NUMBER OF PAGES

16. PRICE CODE
N/A

17. SECURITY CLASSIFICATION OF REPORT	18. SECURITY CLASSIFICATION OF THIS PAGE	19, SECURITY CLASSIFICATION OF ABSTRACT	20. LIMITATION OF ABSTRACT
UNCLASSIFIED	UNCLASSIFIED	UNCLASSIFIED	UL

Infrared Focal Plain Arrays Based on Semiconductor Quantum Dots

E. Finkman and G. Bahir
Department of Electrical Engineering
Technion-Israel Institute of Technology
Haifa, 32000 Israel

January 2002
Final Report
Contract Order No. F61775-00-WE048

The subjects that were studied in the framework of this, including the collaborating researchers in each of them, are detailed below:

1. **"Ultra Small InAs/GaInP/InP Quantum Dots": with Prof. D. Ritter, T. Raz, and D. Gershoni, Technion, Israel**

2. **"InAs/InAlAs/InP Based Quantum Dot Infrared Photodetectors": with J. Brault, and M. Gendry, Laboratoire d'Electronique-LEOM, UMR CNRS 5512, Ecole Centrale de Lion, 69131 Ecully, France**

3. **"Ge/Si Quantum Dots for Infrared Photodetection": with P. Boucaud, V. Le Thanh, and D. Bouchier, Institut d'Électronique Fondamentale, UMR CNRS 8622, Bâtiment 220, Université Paris-Sud, 91405 Orsay, France.**

1. Introduction

In this final report for December 2001 we summarize the progress made at the Technion during the last 15 months. The proposed research topics that were presented to the US Air Force Office in London in the original proposal for September 2000-December 2001 were:

1. Growth of InAs quantum dots (QDs) on various substrates at the Technion using MOMBE growth system of prof. Dan Ritter, and in parallel collaboration with QDs crystal growers from different countries.

2. Characterization of QD layers by optical and atomic force microscopy (AFM) methods.

3. Microfabrication of Quantum Dots Infrared Photodetectors (QDIPs) and electro optics characterization of their device performance.

4. Exploring the possibility to attach detectors matrices to Si based signal processors using In bumps technology.

5. Improvement of the models for assessing device performance.

Our present achievements in the above subjects described, partially, in the last two reports and summarized here. Before going into details we can compare our progress with the research objective presented at the beginning of the research program.

1. Initial efforts to grow InAs quantum dots on strained InGaP layers on InP, using the MOMBE system at the Technion, are successfully giving very unique results. We present some of these results in a short abstract to a conference, which is enclosed in this report (Part 1 of this report). In parallel we continued to work on QD layers provided by collaboration with sources from abroad parts (2 and 3).

1. Quantum dots infrared photodetectors (QDIPs) were implemented and characterized either on InP/InAlAs/InAs or SiGe based QDs layers giving very

interesting and encouraging results were found, including polarized and non-polarized inter-subband front illumination light absorption.

2. As predicted theoretically QDIPs can surpass quantum well infrared photodetectors (QWIPs). Still our fabricated (and also other internationally reported works) and measured QDIPs exhibited performance inferior to that of QWIPs. We suppose that the structural parameters of exiting QDIP layers are far short of optimum. Better understanding of the thermally limited detectivity as function of dot structures, temperature and applied voltage should be studies before we can reach optimum performance.

3. The experimental results, that we have at the end of the program did not justify the originally proposed effort, in the original program, to implement matrices of detectors, which will be attached to Si based signal processors.

Part 1

Ultra Small InAs/GaInP/InP Quantum Dots

The heights of an ensemble of self-assembled InAs/GaAs or InAs/InP quantum dots (QDs) are typically in the range of 10-30 monolayers [1]. Here, we report on InAs QDs grown on tensile strained $Ga_{0.19}In_{0.81}P$ on InP [2], which are just 2-9 monolayers high. The low temperature PL spectrum of the InAs/GaInP/InP dots consists of 7 distinct peaks in the wavelength range of 1.1-1.5 μm, and a broader peak at 1.55 μm. We interpret these distinct peaks as originating from QDs that are exactly 2-9 integer numbers of monolayers high.

The samples were grown by metalorganic molecular beam epitaxy (MOMBE). A 200 nm thick InP buffer layer was grown at 495ºC, followed by a 10 nm thick $Ga_{0.19}In_{0.81}P$ layer, a single layer of InAs quantum dots, and a 50 nm thick InP cap layer. The layers were all grown at 510ºC. Samples grown under the same conditions, excluding the InP cap layer, were scanned by an atomic force microscope (AFM). The dot density, as measured by the AFM, increases gradually with increasing the InAs growth time, from 3×10^8 cm^{-2} (10 sec, see Fig. 1a) to 7×10^9 cm^{-2} (35 sec, see Fig. 1b).

The low temperature PL spectrum of the QDs is shown in Fig. 2. We interpret the peak at ~1 μm as due to carriers recombination within the wetting layer. This peak dominates the emission spectrum in the sample with the lowest density of QDs. In this sample, most carriers recombine in the wetting layer prior to their trapping in the QDs. With increasing the QDs density, emission from the wetting layer drops rapidly, and emission from the QDs increases. The emission spectrum from the QDs consists of up to 7 distinct peaks in the spectral range of 1-1.5 μm, and a broader peak at 1.55 μm. The distinct PL peaks are clearly observed in the spectra from all various samples. Their position is independent of the QDs density. The first peak appears at a wavelength just above the wetting layer emission, and with increasing wavelength the separation between two consecutive peaks decreases.

Distinct peaks in the PL spectrum of QDs are usually attributed to excited states within the QDs. In this case the spectrum varies with incident laser power because

higher energy states are populated at higher excitation powers. Here, by contrast, the shape of the PL spectrum does not change for four orders of magnitude of the exciting laser beam power. We therefore conclude that the discrete PL peaks are due to monolayer variations in the height of the QDs. The wetting layer thickness is estimated to be ~1.5 monolayers, as is found in InAs/InP QDs. The first peak at the shortest wavelength is attributed to about 2 monolayer high quantum dots, the next one to about 3 monolayer high quantum dots, and so on. A similar PL lineshape, consisting of distinct peaks due to monolayer variations in the QD height, was also reported for MOMBE grown InAs QDs on InP [3]. However, with increasing growth interruption time, these peaks disappeared and a broad emission at a longer wavelength evolved. The InAs QDs grown on GaInP reported here retain their discrete height distribution even after a long growth interruption. Moreover, two and three monolayer high dots were not observed in the InAs/InP system [3].

The measured peak energies are compared to the theoretically calculated energies, in fig. 3. The theoretical values were calculated using an 8 band k·P model for InAs quantum wells between $Ga_{0.19}In_{0.81}P$ barrier on one side and InP barrier on the other [4]. A fairly good agreement is evident between the calculation and the position of the QDs emission peaks at high energy (thin QDs). The discrepancy increases with the increase in the number of monolayers. This may be attributed to the increasing importance of the lateral confinement for higher QDs. Diffusion of Ga atoms into the QDs may also contribute to this discrepancy.

It is presently not clear to us, why InAs/GaInP/InP QDs exhibit this unusual discrete height distribution. Few possible explanations are currently under investigation.

References:

1. N. Carlsson, T. Junno, L. Montelius, M.E. Pistol, L. Samuelson and W. Seifert, J. Cryst. Growth **191**, 347 (98).
2. G.M. Cohen, P. Zisman, G. Bahir and D. Ritter, J. Vac. Sci. Technol. B **16**, 2639 (98).
3. P.J. Poole, J. McCaffrey, R.L. Williams, J. Lefebvre and D. Chithrani, J. Vac. Sci. Technol. B **19**, 1467 (01).

4. D. Gershoni, C.H. Henry and G.A. Baraff, IEEE J. Quantum Electron. **29**, 2433 (93).

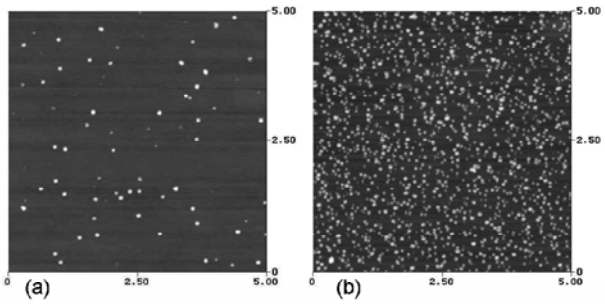

Fig. 1: 5μm × 5μm AFM images of InAs quantum dots grown on $Ga_{0.19}In_{0.81}P$ layers for (a) 10 sec and (b) 35 sec.

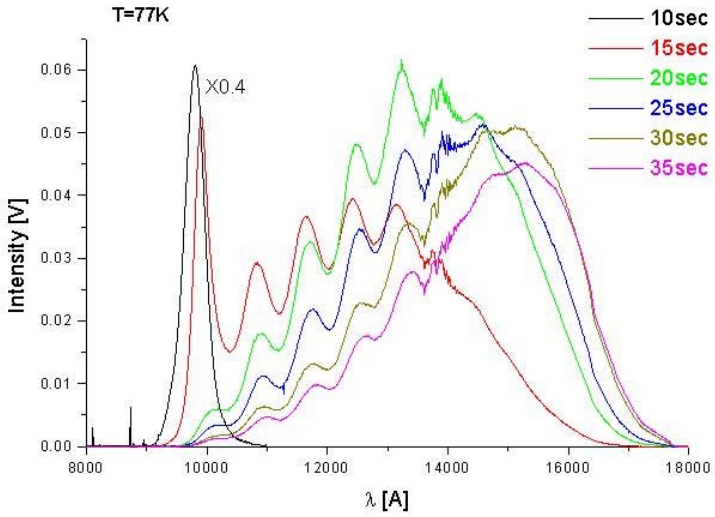

Fig 2: PL spectra obtained at 77 K from InAs/$Ga_{0.19}In_{0.81}P$/InP quantum dots for different InAs growth time.

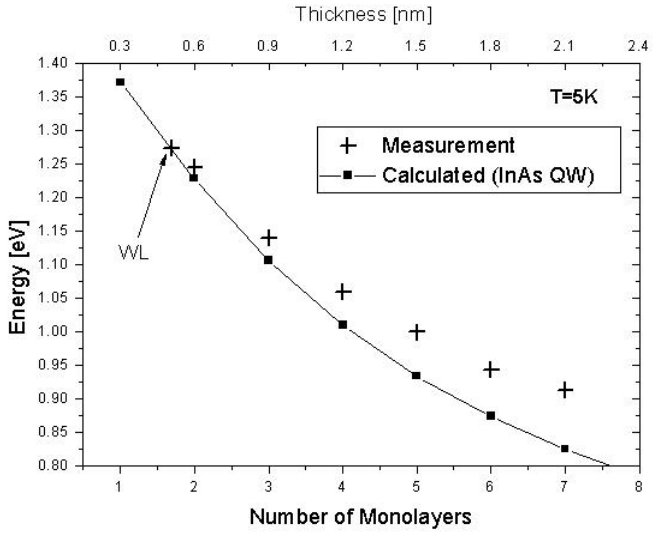

Fig 3: Measured and calculated PL emission energies at T=5K. The calculated values are for an InAs quantum well with $Ga_{0.19}In_{0.81}P$ and InP barriers.

Part 2

InAs/InAlAs/InP Based QDIPs

Introduction

In this work we report on the investigation of photoconductive properties of QDIPs based on self organized InAs quantum dots grown on $In_{.52}Al_{.48}As$/InP(100), using the MBE technique. Dr. Gendry grew the samples at the Ecole Centrale de Lion, Ecully, France. The 3% lattice mismatch characteristic of this material system, which is twice smaller that that of the well studied InAs/GaAs system, allows full coverage of the surface with either quantum wires or enlogated quantum dots aligned along the [1-10] direction depending on the growth conditions. While the First and Second Reports of this program were based on a set of samples with InAs quantum wires characteristics, in this work we focused our study on a new set of samples with elongated dot shape trying to improve the understanding and the performance of QDIPs detectors. Qualitatively the results, between the different samples, are similar but we made here more systematic study. Due to the short time schedule (15 months) of this program we present here the main experimental results of this study where additional analysis will take more time.

Experimental Techniques

The sample growth process was described in detail in Ref. 1. The samples layers structure is shown in figure 1 a. It composed of 10 layers of self assembled InAs dots, separated by 500 Å thick InAlAs (lattice matched to the semi-insulating InP substrate) barrier layers. The barriers were delta doped in their center by Si at a sheet concentration of $2.5\times10^{11}cm^{-2}$. InGaAs contact layers, 5000 Å thick and 10,000 Å thick, n-doped with Si at a concentration of $8\times10^{18}cm^{-3}$, were grown on top and

bottom of the structure respectively. The dots grow in a shape of a parallelepiped with a typical dimension of 500 Å × 300 Å × 20 Å, with their long axis along [1-10] axis, and with concentration of ~ 7×10^{11}cm^{-2}. The structure of this sample is slightly different from the samples previously studied in Reports 1 and 2, where we tried, in the new sample, to reduce the dark current component by decreasing the delta doping in the barrier from 5×10^{11} cm^{-2} to 2.5×10^{11} cm^{-2} and by introducing 1000 Å InAlAs barrier, instead of 250 Å, between the bottom contact layer and the first QDs layer.

The InAs nano-structures characterized, by the crystal grower, using atomic force microscopy (AFM), PL and IR spectroscopy (Ref. 1). Figure 2 shows atomic force microscope images of uncapped InAs islands of the two different samples: sample (a) is a typical image of the samples used for Reports 1 and 2. Sample (b) elongated dots are an image of the last growth process. The quantum dots were investigated by the absorption and photocurrent spectroscopy. Fig. 3 shows the room temperature photo-induced infrared absorption spectrum at normal incidence of undoped sample (with the same structure as the QDIP sample without contact layers) for light polarized along the [110] and [1-10] crystallographic axis. The single intraband absorption resonance peak, which is shown in Figure 3, is strongly polarized in the plane as consequence of the quantum confinement along the [110] direction. This transition is ascribed to an intraband transition in the dot conduction band between levels confined in the [110] direction, i.e. the smaller in plane confinement direction. Mesa structure detectors were fabricated with an area of 200×200 μm^2. 50×50 μm^2 Ti/Au contacts were evaporated on the InGaAs contacts layers (see Fig. 1 a). Three illumination geometries were used. In the first, normal incidence (front illumination) photoconductive spectra were taken, as function of light polarization relative to [110] defined as the x-axis, in which the electric field is along the width of the dot. The light polarization was changed in steps of 10 degrees between the [110] to [1-10], the y-axis, were the electric field is parallel to the dots length. In the second and third configurations, the samples were cleaved along the [110] and [1-10] directions, and were illuminated through 45º - wedges (Fig. 1a), polished along the two directions, were in these configurations two polarizations of incoming IR beam are possible, for each cleavage line. In the s-polarization (TE), the electric field is parallel to the in plan x or y axis's. In the polarization (TM), due to the 45º wedge, 50% of the component of electric field is along the growth direction, z axis, and 50% is in plan

along x or y axis's. Besides, all spectra were taken as function of temperature between 15 K and 100K, and as a function of bias. In the following paragraph we will present the main experimental result of our study.

Experimental results

The photoconductive spectra presented here were obtained using a Mattson Cygnus FTIR for various biases polarizations and temperatures. Figure 4 shows front illumination spectra as function of bias at 15 K. Figure 5 shows front illumination spectra as function of polarization angle between [110] to [1-10] and Fig 6 shows the front illumination spectra as function of temperature. The dot asymmetry and the 3 D confinement remove the degeneracy of the eigenstates, and also alleviated the polarization selection rules, which prohibits intersubband absorption of radiation at normal incidence in quantum well. Two main peaks are observed, one at 90 meV, and other around 250 meV. The intensity of the first peak increases super linearly with bias (Fig. 4) indicating a bound-to-bound transition followed by tunneling into the continuum. The second peak is linearly dependent on bias, typical for bound to continuum transitions. The low energy peak is completely polarized along the [1-10] direction (Fig. 5), which suggests, again, that this is transition between two discrete electronic levels in the dot conduction band. Exploitation of infrared polarization signatures can enhance the contrast of targets vs backgrounds. Targets are composed of man made materials that tend to be smoother than natural materials, and hence reflect and emit stronger polarization signature than natural background. The temperature dependence of the integrated signal (Fig. 7) signal shows a striking difference between the two peaks. While the resposivity of the 90 meV peak decreases linearly with raising temperature from 18 K to 70 K, which of the second stays practically constant. We are working now on a model, which is based on two competing mechanisms, which are controlling the exited level population to explain this temperature effect. Different spectra are seen if we take it throw the wedges illumination either through [110] or [1-10] (Figures 8 and 9). A new peak, at about 160 meV, emerge either in the two wedge illumination configurations. In Report 2 we attributed this third peak to plasma frequency effect when the IR beam is wave guided in wedge illumination configuration. This issue is under study now. The dark current

of this structure is very asymmetric and similar to pn junction dark current (Fig. 10). Comparison of forward and reverse bias dependence of the three photoconductive peaks (Fig. 8 and Fig. 9) shows a striking difference between the low energy peak (90 meV), which disappear at low forward bias, and the two higher energy peaks. We attribute these effects to the asymmetric structure of our QDIP sample.

Summary

In conclusion, we presented a detailed photoconductive study of intraband transition in self-assembled quantum dots. We demonstrated multicolor photoconductive spectra. In contrast to QWIP, which prohibits detection at normal incidence, QDIP's allow detection at front illumination, which is comparable in intensity to that of incidence parallel to the layers. Front illumination polarization sensitive detection was demonstrated which could improve target to background detection. In spite of the expectations to observe higher detectivity (compared to QWIP) due to the phonon bottleneck none of our sample has shown such performance. This issue still should be study.

References

1. F. Fossard, F. H. Julien, E. Peronne, A. Alexandrou, J. Brault, M. Gendry, Infrared Physics & Technology; **42**, 443 (2001).
2. E. Finkman, S. Maimon, V. Immer, G. Bahir, S. E. Schacham, F. Fossard, F. H. Julien, J. Brault and M. Gendry, Phys. Rev. **B 63**, 0455323 (2001).

Figure 1. (a) Detector structure and illumination configurations. (b) AFM image of uncapped sample with axes definition.

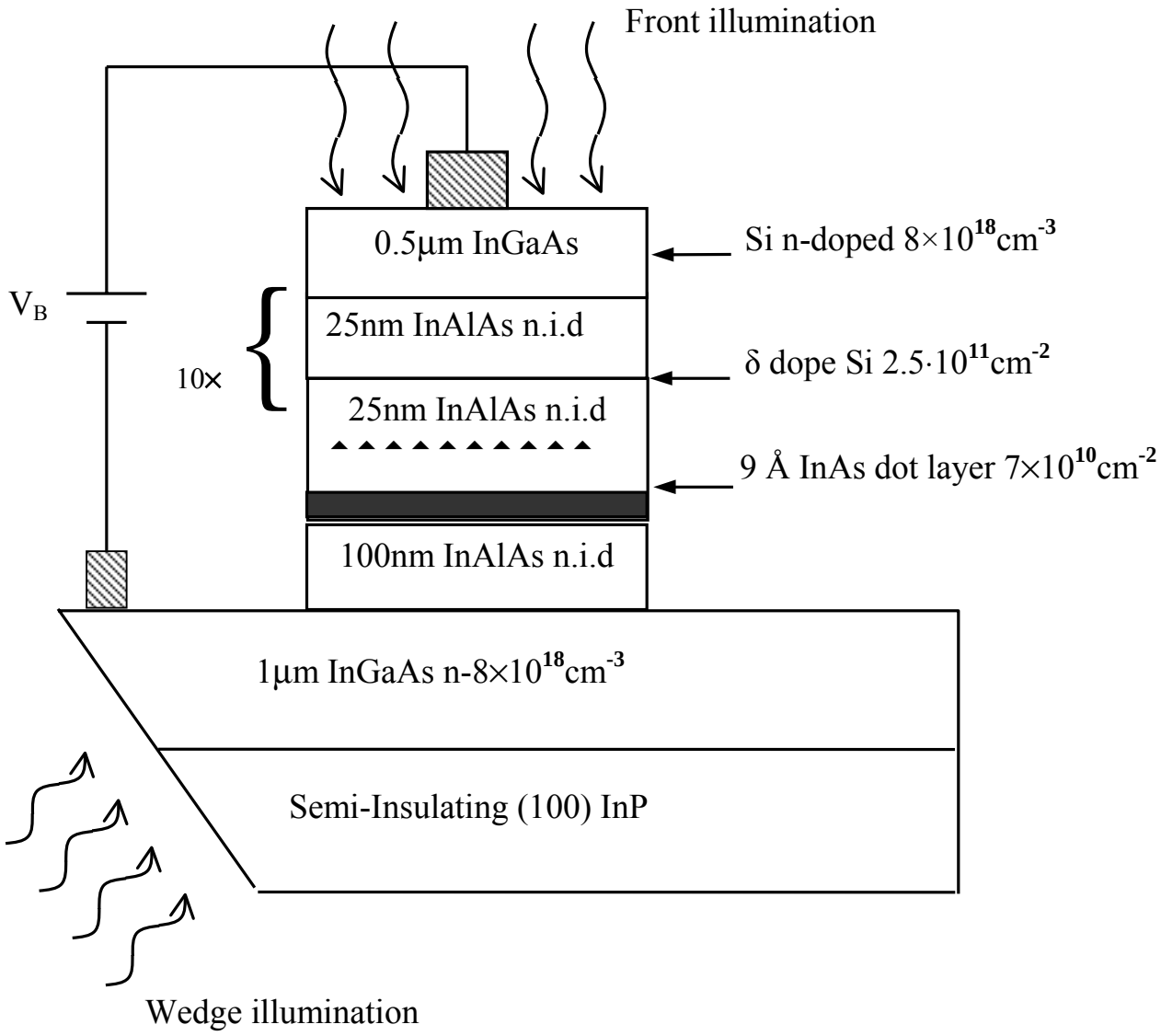

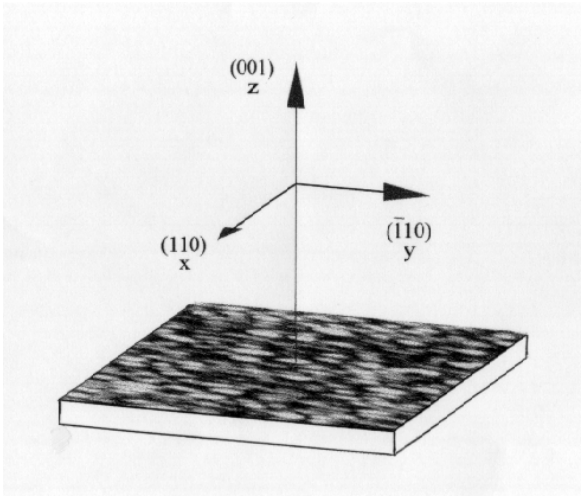

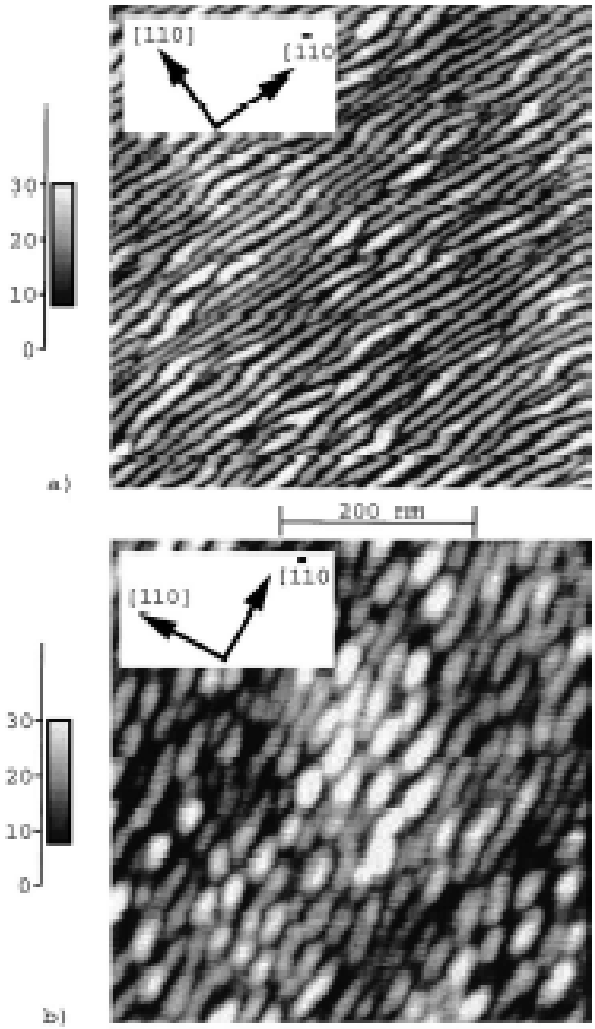

Figure 2 Atomic force microscopy of uncapped sample containing (a) InAs wires, (b) InAs enlogated dots.

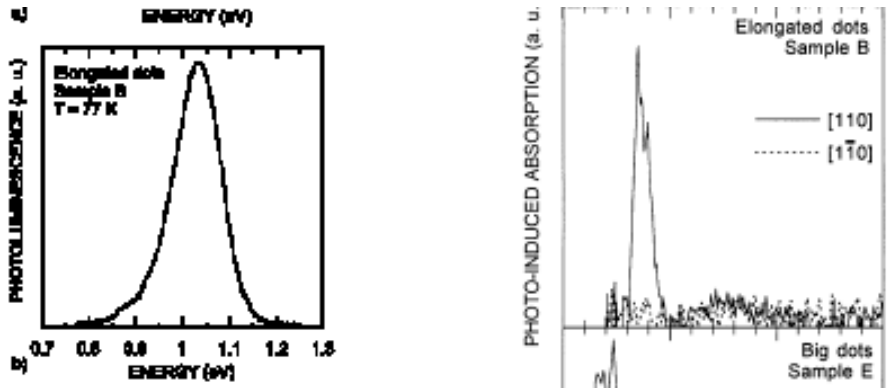

Figure 3. (a) 77 K PL of undoped sample containing 10 planes of InAs dots
(b) 300 K photo-induced absorption of sample containing 10 planes of InAs dots.

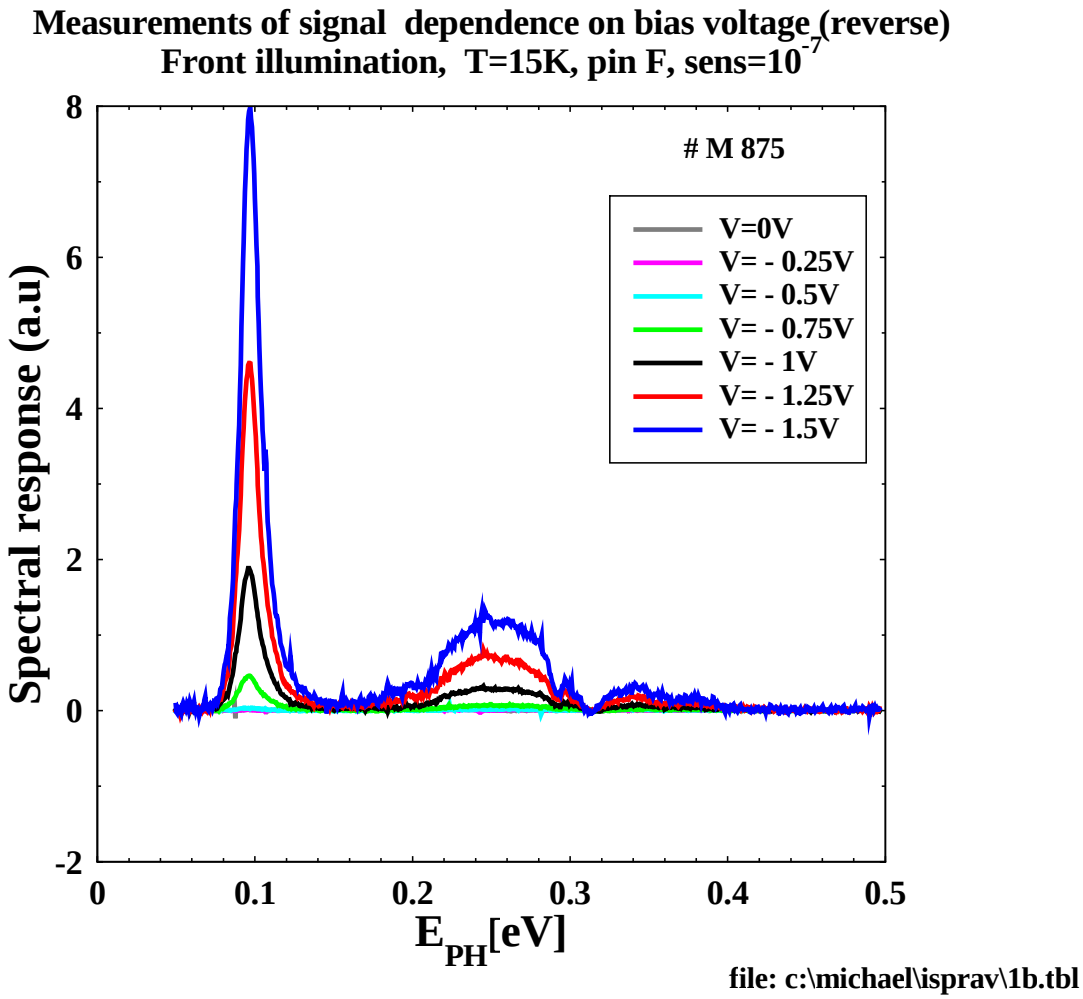

Figure 4. QDIP photoconductive front illumination spectra at 15 K as function of reverse bias.

al, front illumination, as function of polarization

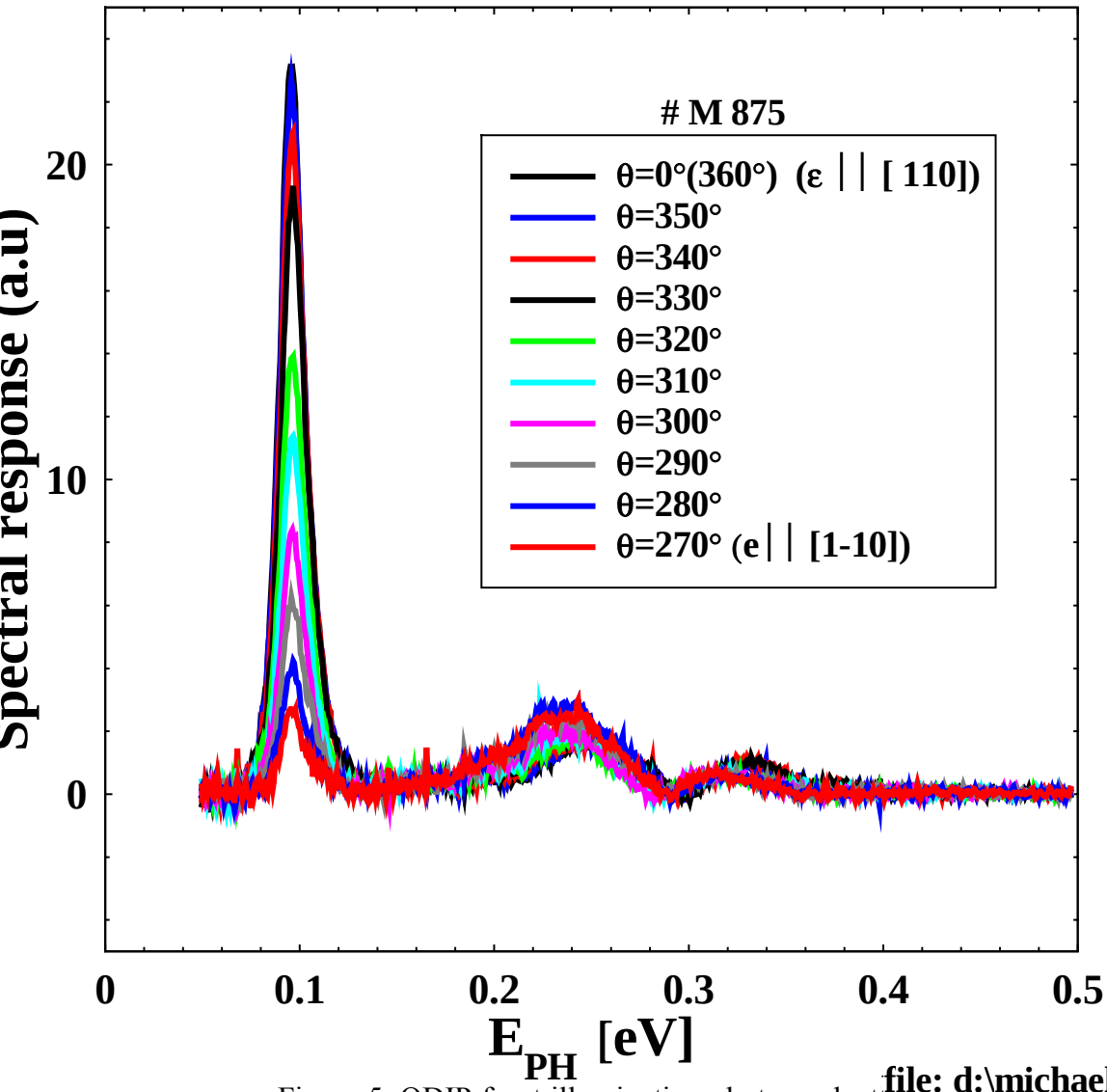

Figure 5. QDIP front illumination photoconductive spectra at 15 K as function of polarization angle. The low energy peak is polarized while the high energy peak signal is not depend on polarization angle.

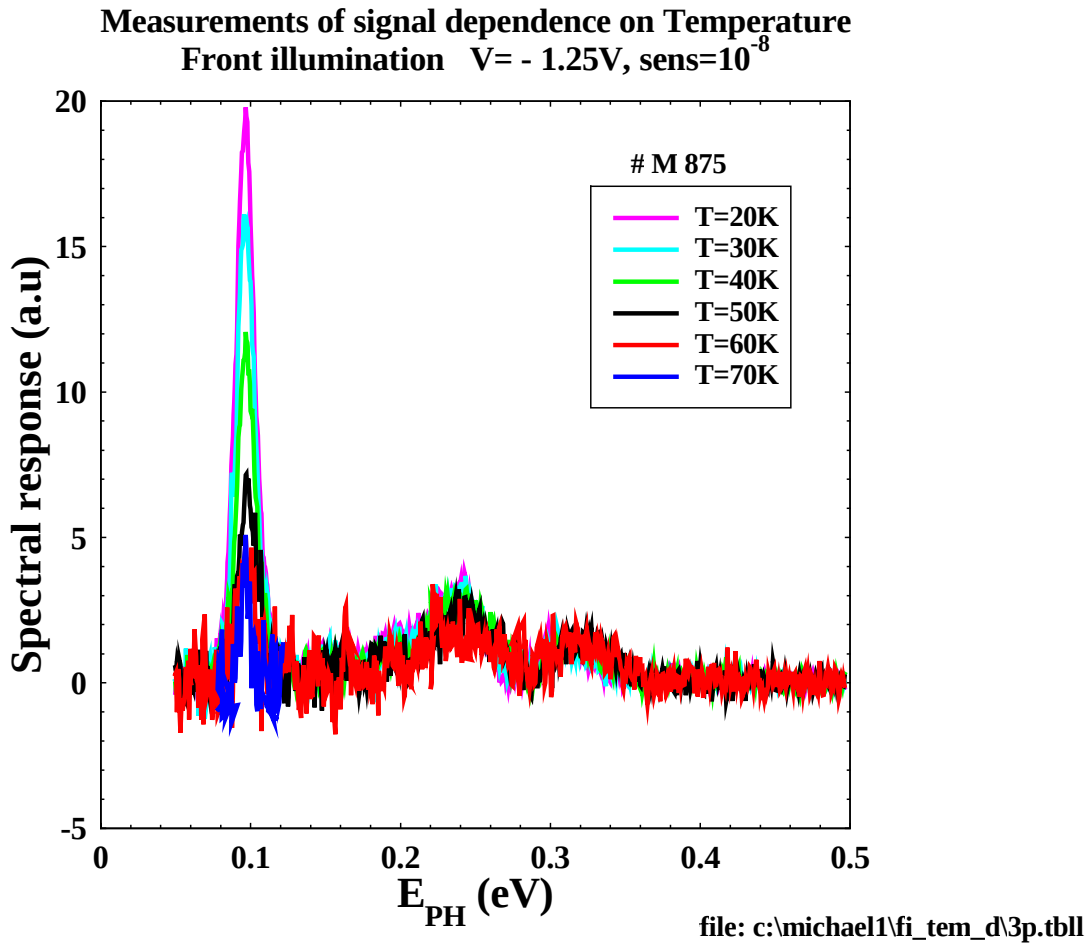

Figure 5. QDIP spectra in front illumination and reverse bias as function of temperature.

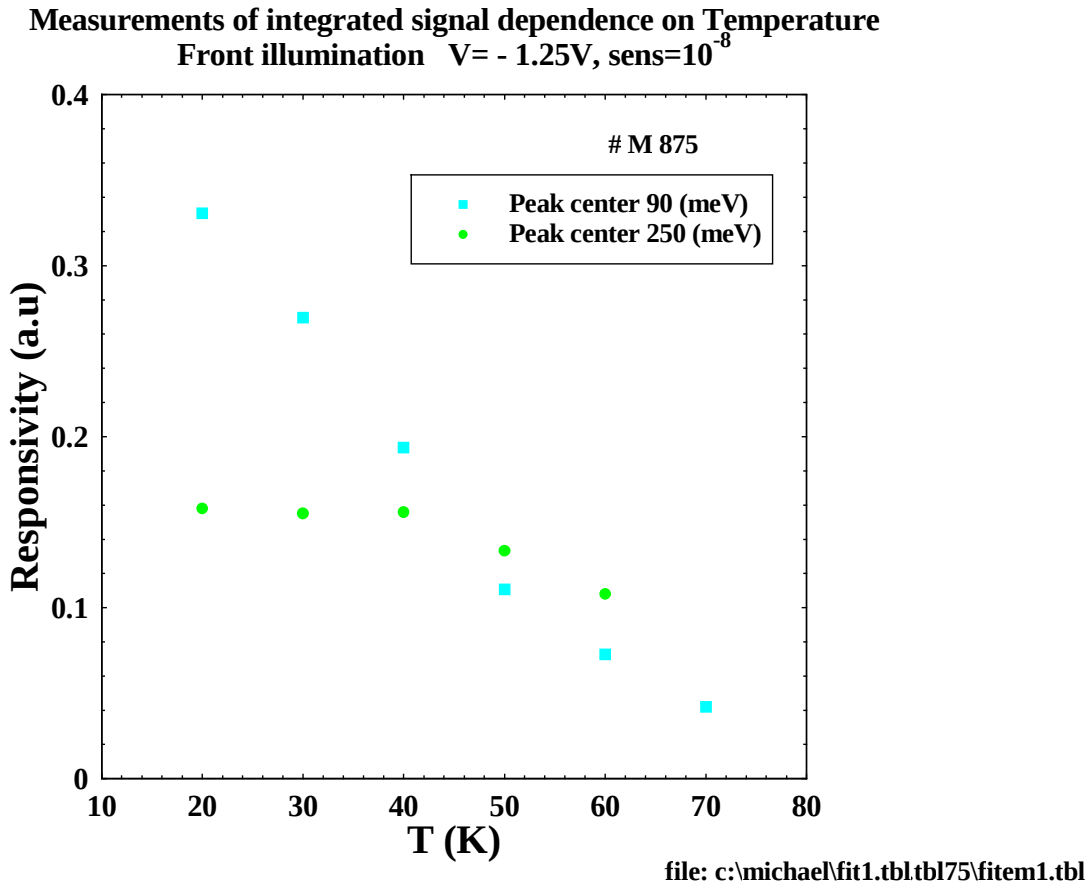

Figure 7. QDIP front illumination integrated spectra as function of temperature.

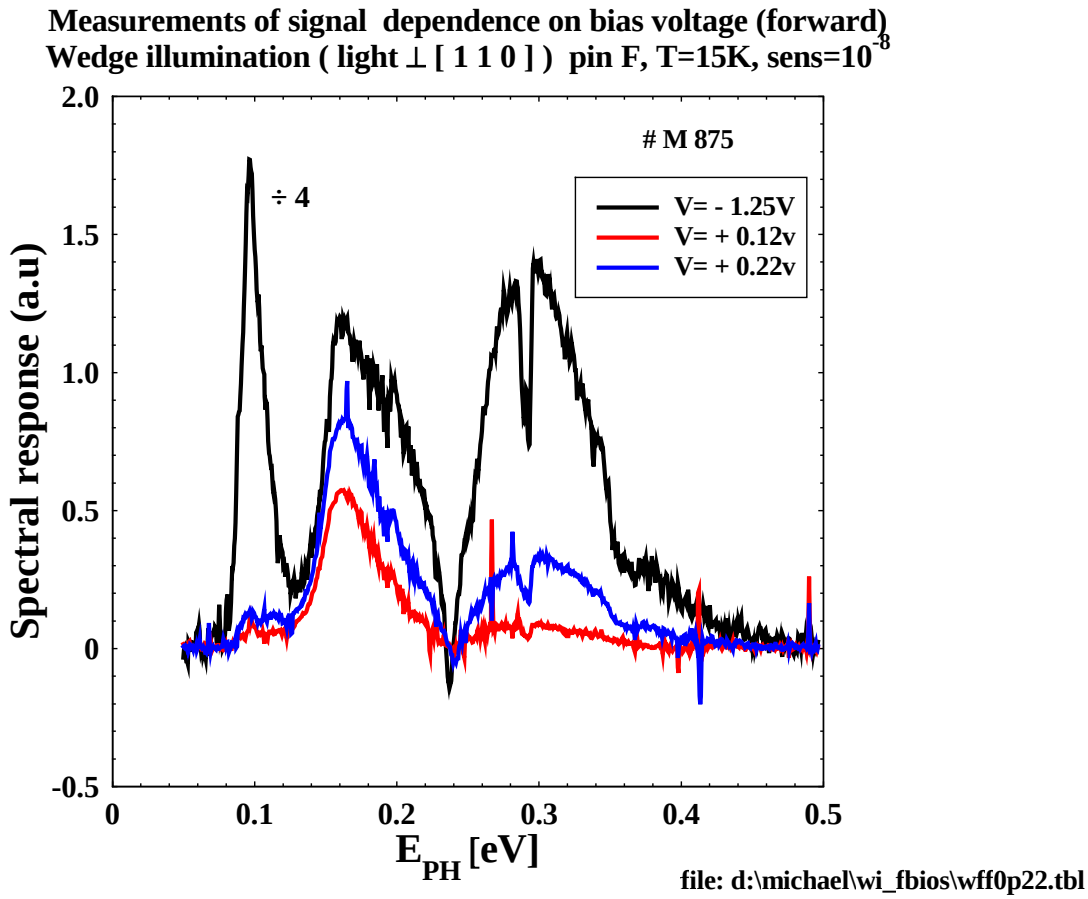

Figure 8. QDIP wedge [110] illumination as function of bias.

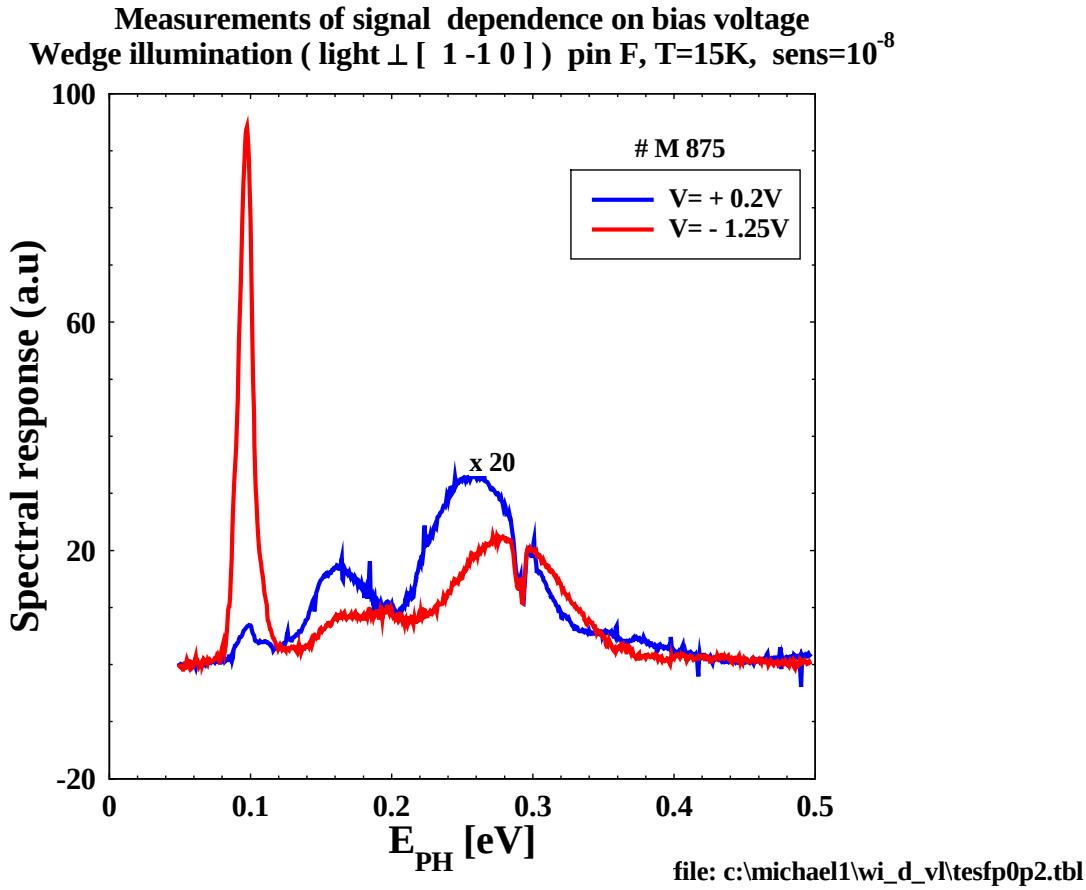

Figure 9. QDIP wedge [1-10] illumination as function of bias.

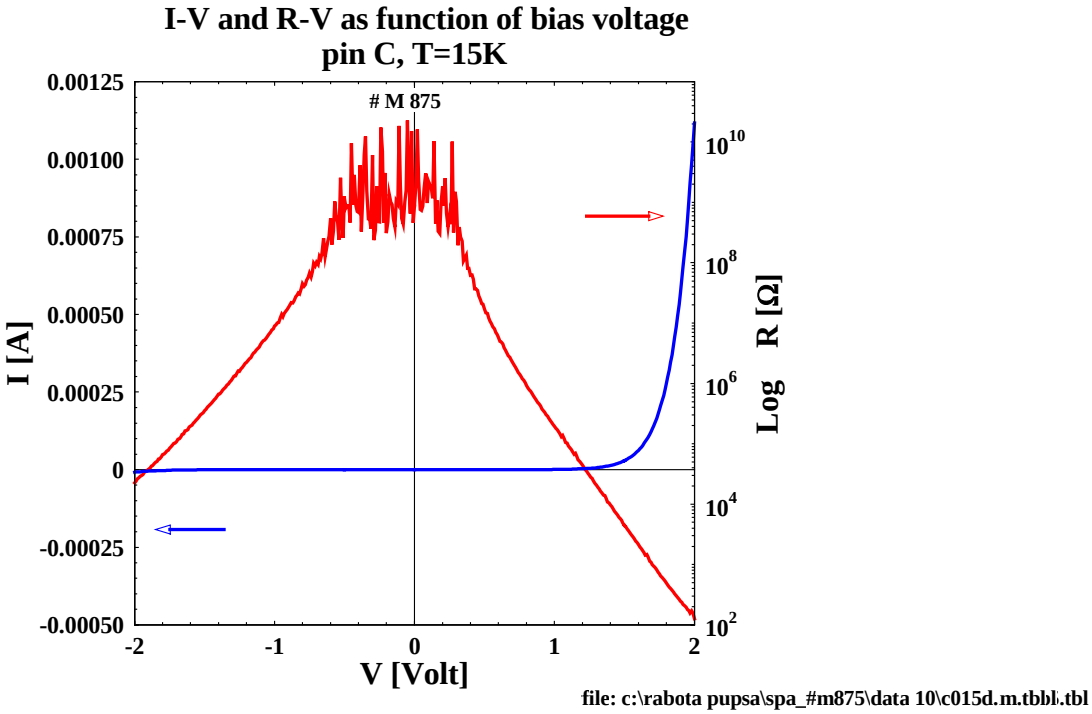

Figure 10. Dark current and dynamic resistance of QDIP structure at 15 K

Part 3

Ge/Si self-assembled quantum dots for infrared photodetection

1. Introduction

One advantage of using quantum dots instead of quantum wells relies on an expected larger photoconductive gain associated with a reduced capture probability. Another advantage is related to the nonvanishing normal incidence absorption which can be observed in quantum dots.[a,b]

The objective of this project was to investigate the realization of new devices based on nanostructures for infrared photodetection. We have chosen to study *self-assembled* Ge/Si semiconductor quantum dots (QDs), and to implement quantum dot infrared photodetectors (QDIPs) that are based on intraband (intersublevel) transitions between the confined hole states. The use of Ge/Si quantum dots exhibits three advantages:

i) The realization of self-assembled quantum dots is inherent to the growth process, with no need of additional pre, or post growth techniques. Thus, it is the simplest way to realize a device with three-dimensionally confined heterostructures. Si-based self-assembled quantum dots can be easily obtained using the Stranski-Krastanow growth mode between lattice-mismatched Ge and Si.[c,d,e] The 4.2 % lattice mismatch between Ge and Si leads usually to the formation of islands with a small aspect ratio (height/base width).

ii) The performances of quantum dots for infrared photodetection can be intrinsically enhanced as compared to quantum well infrared photodetectors (QWIP) due to the longer relaxation time of carriers inside the quantum dot. The longer relaxation time is a direct consequence of the discrete density of states associated with the 3D confinement potential in quantum dots. Besides, one expects a decrease of the carrier capture efficiency for quantum dots as compared to quantum wells since the dots cover a smaller surface as compared to the wells. These effects should lead to an increase of T_{BLIP} (temperature at which the noise of the detector is dominated by the fluctuation of the background photons).

iii) Ge/Si self-assembled quantum dots are compatible with Si-based signal processing, thus allowing an easy integration of the devices with CMOS read-out circuitry. The monolithic integration with Si-based electronics is expected to avoid such problems encountered for large-area infrared focal plane arrays like the thermal mismatch between III-V and IV-IV materials. It is worth noting that in the case of pseudomorphic SiGe grown on Si, a significant valence band offset exists between both strained and relaxed Ge on Si. The existence of this valence band offset leads to the realization of p-type devices either for quantum dots or quantum wells. Si-based valence band intersubband photodetectors using SiGe quantum wells were demonstrated in the past years.[f,g,h]

2.1 Photoconductive QDIP measurements

Five quantum dot wafers were grown, processed, and characterized. Each containing 10 or 15 periods of active doped layers, and Si doped contact layers on bottom and top of the heterostructures. A detailed layer structure of 3 of them is given in Figure 9. For the purpose of analyzing the following results we summarize below the relevant differences in their design parameters:

1. A206 – with modulation delta doping of $5x10^{16}$ cm^{-3} 2 nm away from the dot layers. Dot concentration $2\text{-}3x10^{9}$ cm^{-2}. (Intended 2 carriers per dot).
2. A203 – same as A206, including Si contact layers but undoped otherwise.
3. A263 – similar to A206, except that only wetting layers were grown (with no dots).
4. A 266 – similar to A206 except that lower growth temperature (570 °C) as compared to the other samples (600-620 °C) in an attempt to achieve smaller, and more uniform, dots[11].The photoluminescence of the quantum dots in this sample had a lower magnitude as compared to the others.
5. A410 – similar to A206 with much higher delta doping of $5x10^{18}$ cm^{-3}. 15 periods
6. A411 – same doping amount as in A410, but directly in the dot layers. 15 periods

Measurements were performed on wedged samples and were taken at different applied voltages, with S and P polarization measurement for each voltage. The spectra

that are presented in the figures of this section are normalized photocurrent spectral response graphs. That is to say that the result for each photocurrent measurement was divided by the applied voltage and by the applied gain of the current amplifier (see setup in Fig. 12). This is done in order to be able to visualize the relative voltage dependence of the peak intensity – linear, sub-linear or super-linear. In the case of linear peak behavior the normalized peaks will be of the same magnitude, in sub-linear behavior the higher voltage normalized peak will be smaller in magnitude and in super-linear behavior it will be higher. Understanding the peak behavior is important since it reflects on the optical transition mechanism involved, as will be discussed below.

Samples A203 and A263 were grown for reference purposes. A203 was used to check the quality of the growth process, and to investigate the properties of the nanostructures. QDIPs were implemented and measured on A263 in order to ascertain that the origin of the infrared PC signal stems from the dots. No detectable photoconductive signal was found on A263.

Figures 1-2 show the normalized photocurrent spectral response for selected positive voltages for samples A206. Results of A266 are not presented since the performance of its detectors was inferior to that of those implemented on the other 3 wafers (A206, 410, 411) (presenting much lower responsivity, and much higher noise). The reasons are still not clear. Its spectral features, however, were similar to those of the other samples. Positive voltage in the figures refers to mesa potential is positive relative to the common contact.

The figures show the superposition of such spectra for several applied voltages. The spectral response consists of a broad multipeak. Two clearly noticeable peaks are resolved at low voltages around 115 and 155 meV. A little less noticeable but still visible peak is observed around 220meV. A strong peak emerges around 90meV, and a shoulder around 70 meV suggests the existence of a fifth peak around that value.

When the bias voltage is increased, the intensity of the low energy peaks is increasing faster than those at the higher energies. The 90meV peak is the dominant one at the highest voltage attained (+3V).

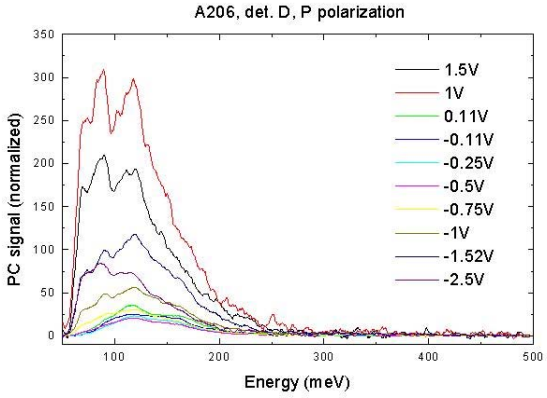

Figure 1(a) : Photocurrent spectral response at 18°K of sample A206 for P polarization; from –2.5V to 1.5V.

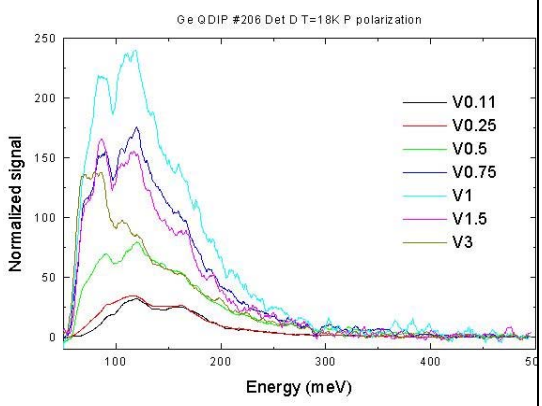

Figure 1(b) : Photocurrent spectral response at 18°K of sample A206 for P polarization; from 0.11 to 3V.

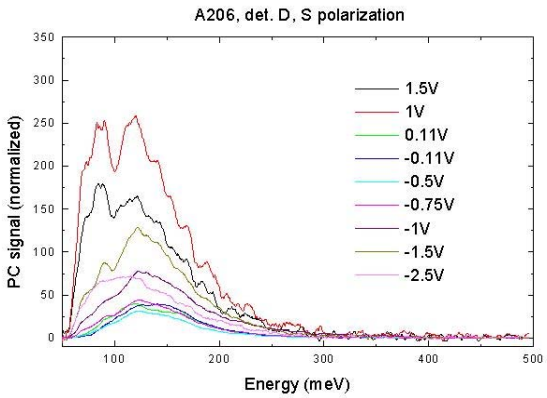

Figure 2(a): Photocurrent spectral response at 18°K of sample A206 for S polarization; from –2.5V to 1.5V.

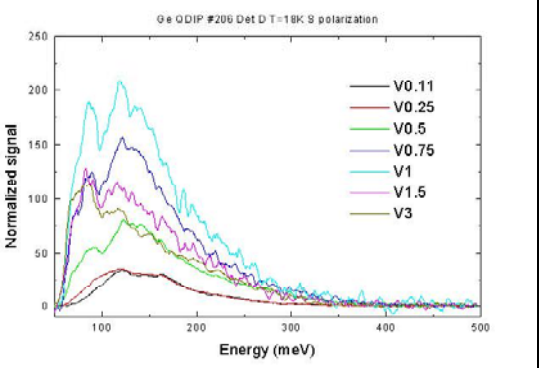

Figure 2(b): Photocurrent spectral response at 18°K of sample A206 for S polarization; from 0.11 to 3V.

The steep decline of the spectral response in the lower limit of the graph is due to phonon absorption in the Si.

2.2 Measurements and BLIP performance

Figure 3 shows an IV curve of the A206 device measured at 17°K while the wedge was exposed to room temperature radiation, superimposed on several measurements taken with a cold shield at different temperatures. We can conclude

from this figure that the device operates as a BLIP at around 20°K. Similar curves are shown for detectors implemented on A410 and A411 in figures 4 and 5, respectively.

The results indicate again a BLIP temperature of around 20°K for both detectors. However, the dark currents show large differences between the three detectors when compared at the same temperatures. With those of A206 and A410 of about the same order of magnitude, and that of A411 about 2 orders of magnitude less. This should imply that A411 would present an order of magnitude less noise, and much better TBLIP, which is not observed. The contradiction is still under study (A411, processed in late January, is still being measured).

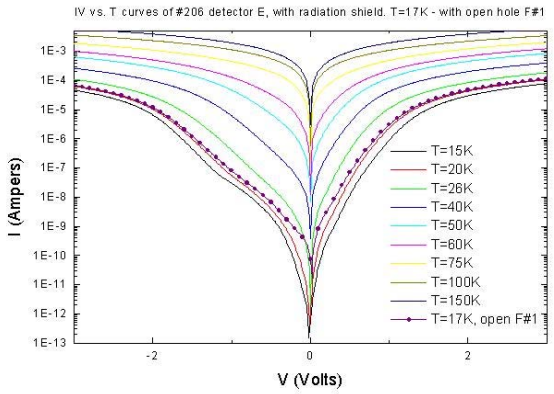

Figure 3 : IV curves of A206 detector E as a function of temperature, with cold shield and with 17°K cold detector exposed to an opening in the cold shield with F#1 aperture, exhibiting BLIP performance up to about 20K

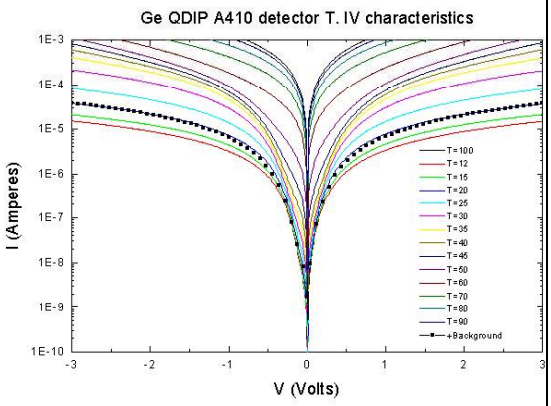

Figure 4 : IV curves of A410 detector T as a function of temperature, with cold shield and with 17°K cold detector exposed to an opening in the cold shield with F#1 aperture

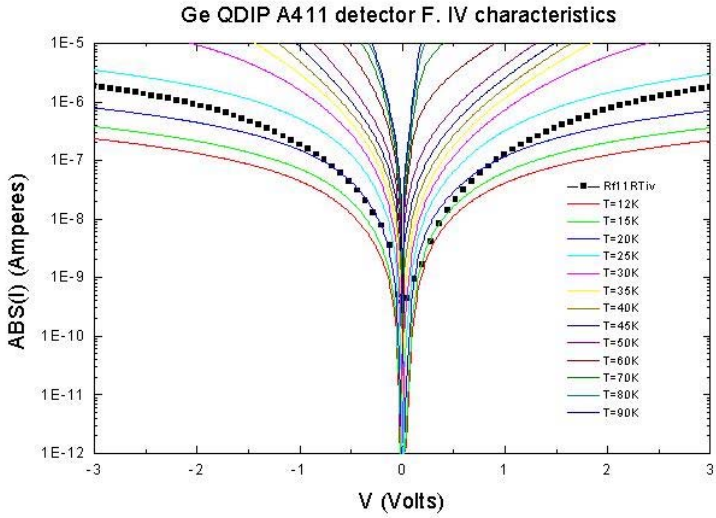

Figure 5 : IV curves of A411 detector E as a function of temperature, with cold shield and with 17°K cold detector exposed to an opening in the cold shield with F#1 aperture

3. Conclusion and perspectives

We have successfully designed and realized some new infrared photodetectors with Ge/Si self-assembled quantum dots. The operation of the detectors implied the control of the growth and of the doping of Ge/Si islands by chemical vapor deposition. The electronic structure of the quantum dots has been investigated by optical techniques (photoluminescence, photo-induced infrared absorption). We have performed some three-dimensional calculation of the confined hole states in the dots. The key results of the research performed at IEF have been :

- Growth and doping of high-quality Ge/Si self-assembled quantum dots
- Control of the dot dispersion for multilayers
- Measurements of the dot composition
- First observation of the interband recombination associated with the excited states in the islands
- First observation of the intersublevel absorption in Ge/Si quantum dots

The Technion has successfully processed the samples and performed the electrical and optical characterizations. Several types of detectors were studied. The key achievements are:

- Design of Ge/Si quantum dot heterostructures suitable to implement QDIPs
- Developing a microelectronic process to implement such detectors
- Observing a photoconductive signal
- Extensive characterization of Ge/Si QDIPs
- First observation of bound-to-bound transitions by photoconductivity
- In depth analysis and interpretation of the results, including **k·p** 8 band calculations are performed and will be published later.

Quantum dot infrared photodetectors are predicted to have some important advantages over QWIPs like lower dark current, higher internal gain, and normal-incidence response. Their capability for normal incidence absorption was proven in quite a number of studies, including the present one. But most of the other features predicted theoretically were not obtained yet and will require further optimization of the devices.

The dark current limits the performance of this first generation of Ge/Si QDIPs. Direct doping in the dot layer proved to be one way of reducing this phenomenon. It seems that delta doping in the barriers creates internal electric fields that facilitate the thermally assisted emission of holes from the dots to increase the dark current. This is demonstrated by the much smaller dark current in A411 compared to that of A410, and A206. Another possibility is the engineering of new injectors with SiGe alloys instead of Si that should decrease significantly the dark current in the structures and enhance the performances. The SiGe injectors with a lower band gap as compared to Si would be equivalent to GaAs injectors followed by AlGaAs barriers. We will continue our work towards this direction. The collaboration between the IEF group and the Technion is also still in progress for InAs/GaAs QDIPs. It is also interesting to note that intersubband electroluminescence from silicon-based quantum cascade structures was reported very recently.[i] We propose to continue to investigate the Ge/Si self-assembled quantum dots for infrared emission. This research could lead to the demonstration of a silicon-based quantum dot laser.

Besides these future developments on the midinfrared properties of Ge/Si self-assembled quantum dots, the near-infrared properties of the islands appear also very promising for optoelectronic devices. Based on the experience for the growth of quantum dots obtained during these last two years, the IEF group has initiated the development of electroluminescent diodes emitting around 1.5 μm wavelength and quantum dot near-infrared photodetectors. These devices on Si are more specifically developed as an alternative of III-V materials for optical interconnects between chips (intra-chip or inter-chips). This work is supported by **STMicroelectronics** as an industrial partner. First results in this direction have already been obtained.

References

[a] H. Drexler, D. Leonard, W. Hansen, J. P. Kotthaus, and P. M. Petroff, Phys. Rev. Lett. **73**, 2252 (1994).

[b] S. Sauvage, P. Boucaud, J.-M. Gérard, and V. Thierry-Mieg, Phys. Rev. B **58**, 10562 (1998).

[c] D. E. Eaglesham, and M. Cerullo, Phys. Rev. Lett. **64**, 1943 (1990).

[d] P. Schittenhelm, M. Gail, J. Brunner, J.F. Nützel, and G. Abstreiter, Appl. Phys. Lett. **67**, 1292 (1995).

[e] V. Le Thanh, P. Boucaud, D. Débarre, Y. Zheng, D. Bouchier, and J.-M. Lourtioz, Phys. Rev. B **58**, 13115 (1998).

[f] J. S. Park, R. P. G. Karunasiri, and K. L. Wang, Appl. Phys. Lett. **61**, 681 (1992).

[g] R. People, J. C. Bean, S. K. Sputz, C. G. Bethea, L. J. Peticolas, Thin Solid Films **222**, 120 (1992).

[h] P. Kruck, M. Helm, T. Fromherz, G. Bauer, J. F. Nutzel, and G. Abstreiter, Appl. Phys. Lett. **69**, 3372 (1996).

[i] G. Dehlinger, L. Diehl, U. Gennser, H. Sigg, J. Faist, K. Ensslin, D. Grützmacher, E. Müller, Science **290**, 2277 (2000)